Fabrication of Sr_2TiO_4–TiO_2 heterojunction photoanode dye-sensitized solar cells applications

S. Wannapop [a, *], J. Sinudom [a], N. Romyen [a], S. Promnopas [b], T. Kaewmanee [c], A. Somdee [a]

[a] *Faculty of Science, Energy, and Environment, King Mongkut's University of Technology North Bangkok, Rayong Campus, Rayong 21120, Thailand*
[b] *Department of Physics and Materials Science, Faculty of Science, Chiang Mai University, Chiang Mai 50200, Thailand*
[c] *School of Materials Science and Innovation, Faculty of Science, Mahidol University, Nakhon Pathom 73170, Thailand*

The Sr_2TiO_4–TiO_2 heterojunctions were synthesized using a reflux method with various concentrations of NaOH. The synthesized heterojunctions were characterized for their morphological and structural properties using SEM, TEM, XRD, and XPS. The optical properties were analyzed using UV-vis DRS. The fabricated heterojunction photoanodes were incorporated into dye-sensitized solar cells (DSSCs) devices, and their photovoltaic performance was evaluated under simulated sunlight. Our results indicate that the Sr_2TiO_4–TiO_2 heterojunction photoanode fabricated at a pH of 7 and subjected to reflux synthesis at 90°C exhibited the highest energy conversion efficiency among the tested samples.

(Received March 4, 2025; Accepted June 24, 2025)

Keywords: Titanium dioxide, Electrochemical impedance spectroscopy, Nanoparticles, TEM

1. Introduction

Energy shortages are a worldwide concern. Most energy is derived from fossil fuels, which have limited availability. Developing alternative energy sources is crucial. Solar energy is a promising renewable energy source that harnesses the sun's electromagnetic radiation and converts it into electricity [1].

DSSCs are a promising photovoltaic technology owing to their cost-effectiveness, simplicity of fabrication, and high efficiency [2]. Much research has recently focused on improving DSSC performance using new materials and designs. To enhance the efficiency of DSSCs, which are composed of dye sensitizers, photoanodes, electrolytes, and counter electrodes, metal oxides like ZnO [3], TiO_2 [4], and SnO_2 [5] are frequently utilized for the photoanodes. TiO_2 is extensively used as the photoanode in DSSCs because of its beneficial properties, including high electron mobility [6], chemical stability, and biocompatibility [7]. However, despite these benefits, DSSCs face challenges related to efficiency and stability [8], particularly regarding electron recombination [9].

To improve the transport properties of TiO_2 for better solar energy conversion in DSSCs. The morphology, particle size, and pore size of TiO_2 are crucial factors affecting photoelectron diffusion and the overall conversion efficiency of DSSCs. The influence of shape on the performance of DSSCs has prompted the synthesis of TiO_2 nanomaterials in various morphologies, including spherical [10], tubular [11], wire-like [12], rhombic and square shapes [13]. These

* Corresponding author: surangkana.w@sciee.kmutnb.ac.th
https://doi.org/10.15251/JOR.2025.213.377

different shapes are achieved using a variety of synthesis methods. The variations in morphology impact the nanomaterials' crystallite size, band-gap energy, and surface area [14]. Nanoparticles play a crucial role in DSSCs because of their unique properties that greatly enhance the overall performance of the cells. They improve efficiency by maximizing dye loading, enhancing electron transport, and optimizing light harvesting and low-cost-effective solar cells [15]. Several strategies can be employed to enhance the current density of the DSSC photoanode. These include surface modification with blocking layers [16], doping with metals [17], utilizing composite materials [18], improving morphology [19], introducing plasmonic effects [20], optimizing the thickness of the photoanode [21], enhancing material crystallinity [22], and applying chemical surface treatments [23].

Enhancing the efficiency of TiO_2 through the use of blocking layers is an intriguing approach that can boost performance in several ways. These methods can prevent recombination, increase the short-circuit current density (J_{sc}) by reducing electron backflow, improve charge injection, enhance light absorption, and elevate both the open-circuit voltage (V_{oc}), the fill factor (FF) and conversion efficiency (η). Overall, this leads to improved photoelectric conversion efficiency [24]. Very thin TiO_2 coating layers, used as blocking layers (BL), can be made from several materials, including ZnO, SnO_2, perovskite structures, Al_2O_3, and SiO_2 [25]. These layers are produced using various methods, such as spray pyrolysis, sol-gel, dip coating, sputtering, and multi-layer techniques [26];[27];[28]]. Using perovskites as blocking layers provides several advantages, including their wide bandgap and efficient electron transport properties. These materials can minimize interfacial defects, which improves charge separation and reduces recombination [29].

This introduction outlines the reasons for using perovskite as a blocking layer in DSSCs and its potential advantages for enhancing device performance. By incorporating Sr_2TiO_4 into TiO_2, the composite photoanode can broaden the absorption range, thus improving the overall light-harvesting efficiency of DSSCs.

This study provides a comprehensive development and characterization of Sr_2TiO_4–TiO_2 heterojunction for use in DSSCs. This discussion covers various aspects, including synthesis methods, structural and morphological characterization, optoelectronic properties, device fabrication, and performance evaluation of the Sr_2TiO_4-decorated TiO_2-based structures.

2. Experimental

Sr_2TiO_4-TiO_2 heterojunction was synthesized by using the reflux method. First, 0.5 g of Titanium Dioxide (P25) and 0.5 mmol of Strontium Nitrate ($Sr(NO_3)_2$) were dissolved in 50 mL of deionized water and stirred. After thoroughly mixing the solution for 10 minutes, the pH was adjusted using 3 M sodium hydroxide (NaOH) and hydrochloric acid (HCl) to achieve pH levels of 7, 9, 11, and 13. The mixture was transferred to a three-neck flask and synthesized using the reflux method at 90 °C for 1 h. Following synthesis, the products have been washed with DI water and ethanol. The products were dried at 60 °C for 24 h. and calcined at 600 °C for 1 h. The samples were designated as TiO_2, STO-TiO_2-pH7, STO-TiO_2-pH9, and STO-TiO_2-pH11, respectively. The samples were characterized using SEM (JEOL JSM 6335F), TEM (JEOL JEM-2010), XRD (Bruker AXS D8 eco), XPS (Axis Ultra DLD instrument), and UV-vis DRS (Shimadzu UV-2600).

The photoanode was prepared using the sol-gel method. A sample weighing 0.35 g, 0.15 g of PEG, 0.5 ml of DI water, and 0.5 ml of ethanol, was stirred for 30 minutes. The resulting gel was then applied to an area measuring 1.0 cm × 1.0 cm and calcined at 500 °C for 2 hours.

The photovoltaic measurement and electrochemical impedance spectroscopy (ZAHNER elektrik potentiostat) under a solar simulator (Xenon light with AM 1.5G, Newport).

3. Results and discussion

Fig. 1 displays the XRD patterns of commercial P25 and Sr_2TiO_4-decorated TiO_2 at various pH levels. The diffraction pattern of commercial P25 shows two distinct phases: anatase (JCPDS no. 21-1272) and rutile (JCPDS no. 21-1276) [30]. The peak observed at the 2θ angle for STO-TiO_2-pH11 indicates the presence of anatase peaks at positions 25.26°, 37.02°, 37.76°, 38.58°, 48.03°, 53.97°, 55.19°, 62.76°, 68.91°, 70.25°, and 75.13°, corresponding to the anatase structure planes (101), (103), (004), (112), (200), (105), (211), (204), (116), (220), and (215). Additionally, peaks at 2θ positions 27.43°, 36.14°, and 41.21° align with the rutile structure planes (110), (101) and (111). The (114) peak was also detected at position 44.11°, consistent with the tetragonal structure of Sr_2TiO_4 (JCPDS no. 25-0915) [31]. The peak at position 2θ = 44.11°, corresponding to the (114) plane of the Sr_2TiO_4 (STO), increases in height as the pH becomes more essential. Additionally, the diffraction pattern of the Sr_2TiO_4-decorated TiO_2 resembles that of commercial P25, but the pattern for Sr_2TiO_4 appears in conjunction with the TiO_2 pattern.

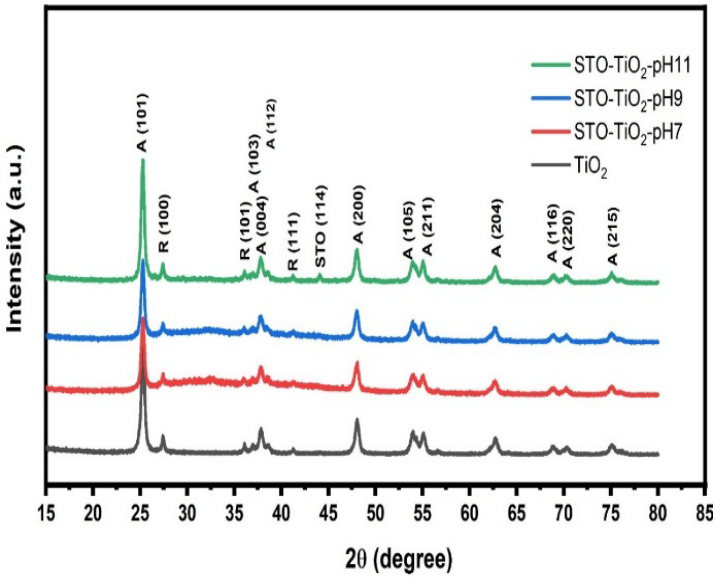

Fig. 1. XRD patterns of TiO_2, STO-TiO_2-pH7, STO-TiO_2-pH9, and STO-TiO_2-pH11, respectively.

The survey spectra for STO-TiO_2-pH7 are presented in Fig. 2a, while the XPS peaks for strontium (Sr), titanium (Ti), and oxygen (O) are illustrated in Fig. 2b to 2d, respectively.

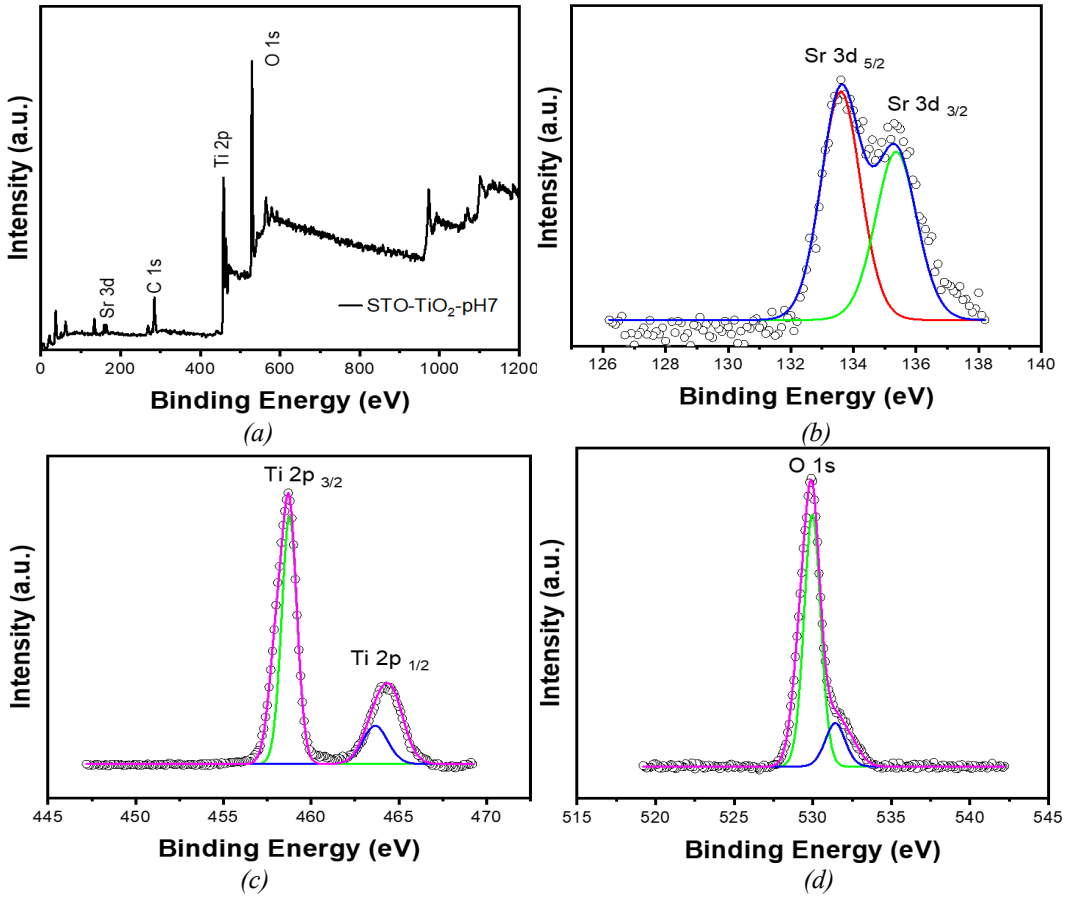

*Fig. 2. XPS survey spectra of STO-TiO_2-pH7 **(a)**, Sr 3d **(b)**, Ti 2p **(c)**, and O 1s **(d)** respectively.*

In Fig. 2b, the peaks for Sr are identified as the spin-orbit split components, Sr $3d_{5/2}$ and Sr $3d_{3/2}$, with binding energies at 133.57 eV and 135.37 eV, respectively. The Ti peak shown in Fig. 2c indicates binding energies of 458.75 eV and 464.62 eV, related to Ti $2p_{3/2}$ and Ti $2p_{1/2}$. [32] Finally, the oxygen peaks depicted in Fig. 2d are found at 529.95 eV and 532.30, corresponding to O 1s. XPS results confirm that Sr_2TiO_4 can decorate the surface of TiO_2, consistent with EDX, TEM, and XRD results.

Fig. 3 shows an SEM image of TiO_2 and the different pH of Sr_2TiO_4 decorated TiO_2. SEM analysis revealed that the pH of synthesis significantly affected the morphology and distribution of Sr_2TiO_4 decorations on TiO_2 nanoparticles. Lower pH levels resulted in more agglomerated morphologies and clustered distributions, whereas higher pH levels led to more uniform morphologies and dispersed distributions. In addition, it was found that the particle size was more significant due to decoration by $S_{r2}TiO_4$ after higher pH levels. Fig. 3f shows the EDX analysis of TiO_2-STO-pH 7, which found the elements Sr, Ti, and O, confirming that the surface of TiO_2 can be decorated with Sr_2TiO_4.

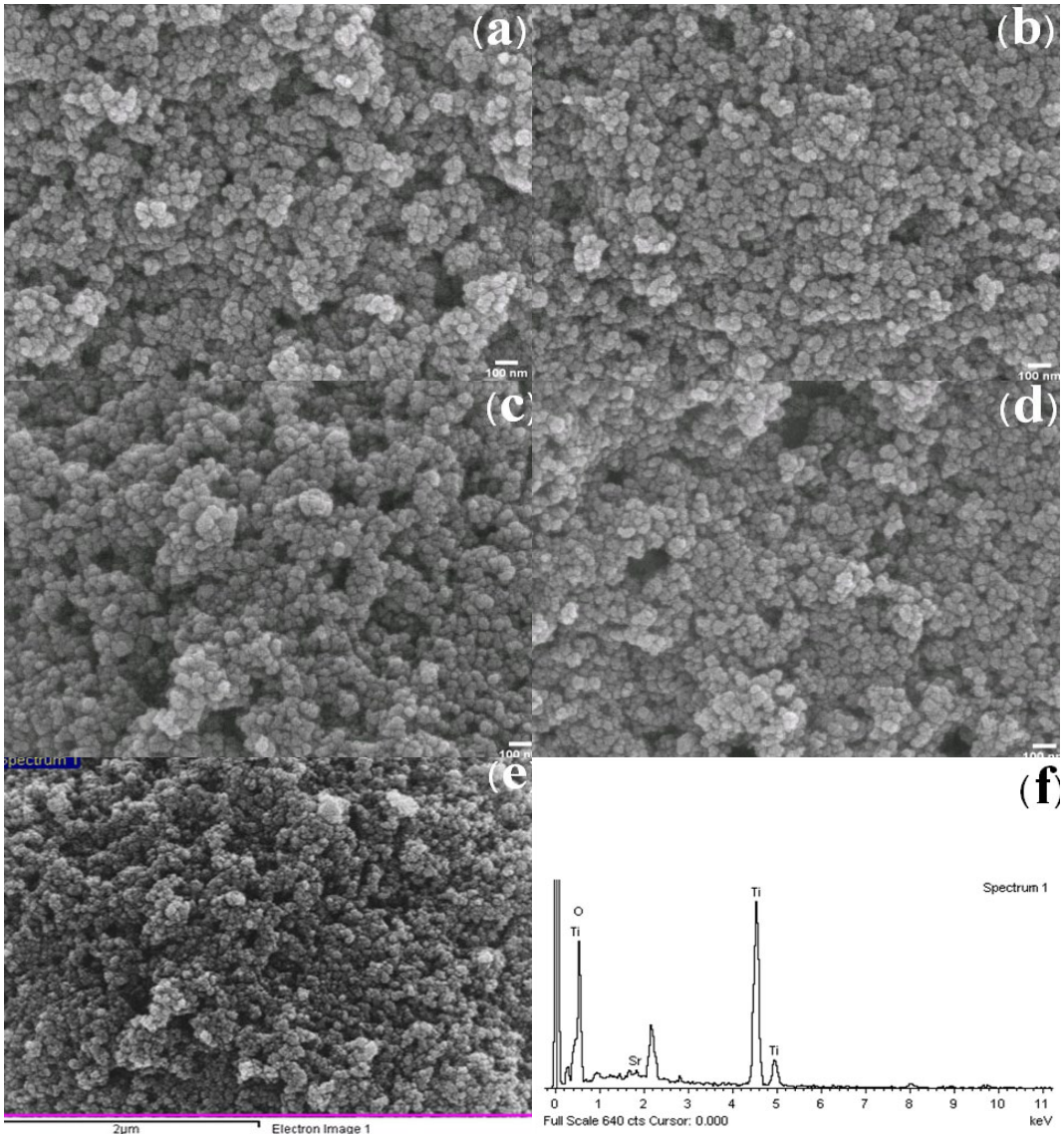

Fig. 3. SEM image and EDX of TiO_2 (a), TiO_2- STO-pH7 (b), TiO_2- STO-pH9 (c), TiO_2- STO-pH9 (d), and TiO_2- STO-pH7 (e-f), respectively.

Comparison and interpretation of the TEM images reveal that the surface of TiO_2 nanoparticles decorated with Sr_2TiO_4, as shown in Fig. 4, is rougher than that of pure TiO_2. The HRTEM for TiO_2 showed the (101) plane of anatase. Following decoration with Sr_2TiO_4, showed the (110) plane of rutile TiO_2 and the (004) plane of Sr_2TiO_4, consistent with the XRD and EDX results.

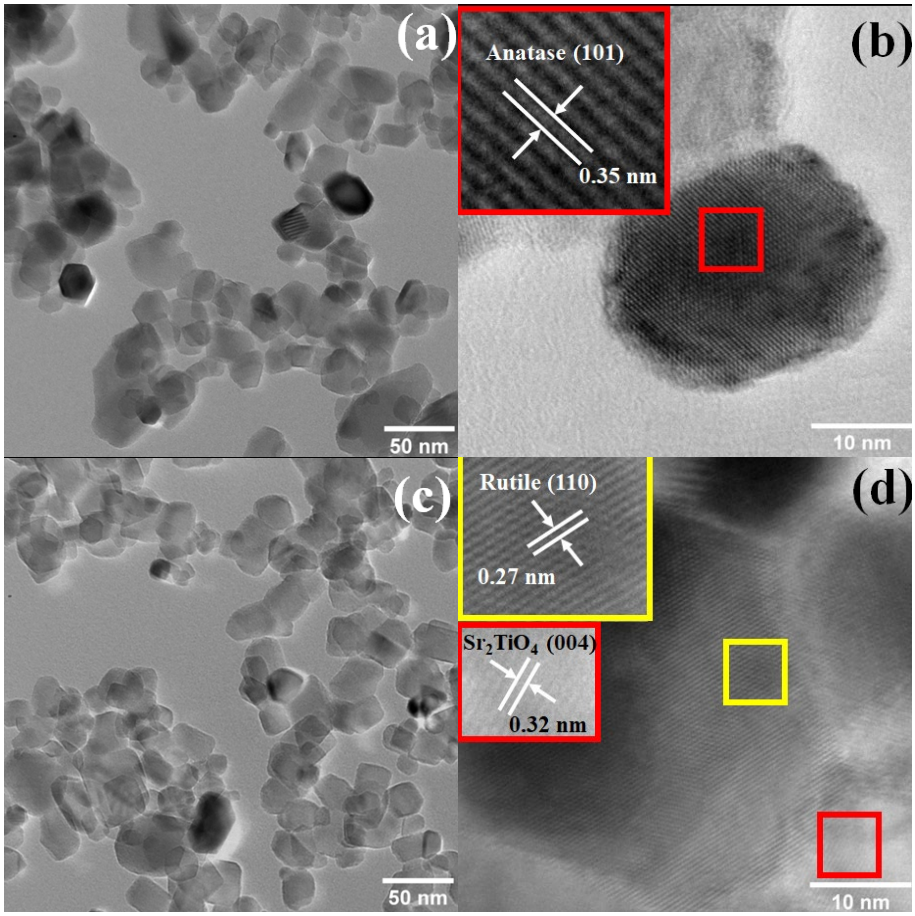

Fig. 4. TEM and HRTEM images of TiO_2 (a-b), and TiO_2- STO-pH7 (c-d), respectively.

Fig. 5a shows the absorption spectra of TiO_2 and Sr_2TiO_4 decorated TiO_2 at different pH levels. A comparison of the UV-vis spectra of samples synthesized with varying concentrations of NaOH reveals that the absorption decreases as the concentration of NaOH increases, corresponding to the XRD result. This is attributed to the more excellent formation of Sr_2TiO_4, which has a wider bandgap than the commercial P25 material. The Tuac plots [33] and direct bandgap values [34] are shown in Fig. 5b. The energy band gaps found for TiO_2, TiO_2-STO-pH7, TiO_2-STO-pH9, and TiO_2-STO-pH11 were 3.12 eV, 3.14 eV, 3.18 eV, and 3.20 eV, respectively.

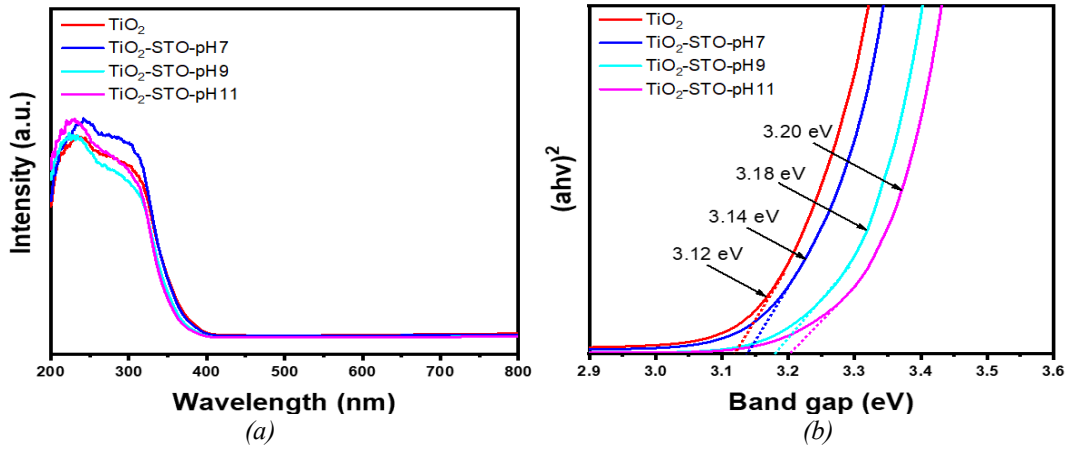

Fig. 5. (a) UV-vis absorption spectra, and (b) Tauc plots of TiO_2 and different pH of Sr_2TiO_4 decorated TiO_2.

The photocurrent density–voltage curves **(J-V)** of DSSC fabricated with the TiO_2 and different pH of Sr_2TiO_4 decorated TiO_2 samples are shown in Fig**.** 6, with the detailed photovoltaic parameter listed in Table 1**.** The TiO_2-STO-pH7 is the highest efficiency achieved with V_{oc}, J_{sc}, FF, and η equal to 620 mV, 1**.**09 mA cm^{-2}, 0.59, 0**.**40**%**, respectively**.** The samples with average particle size around 20-30 nm present similar P25, but the surface is rougher than that of P25**.** It is noted that despite having similar properties to P25-TiO_2, the surface roughness of the samples may influence the performance of DSSC devices, potentially contributing to variations in photovoltaic parameters**.** [35]

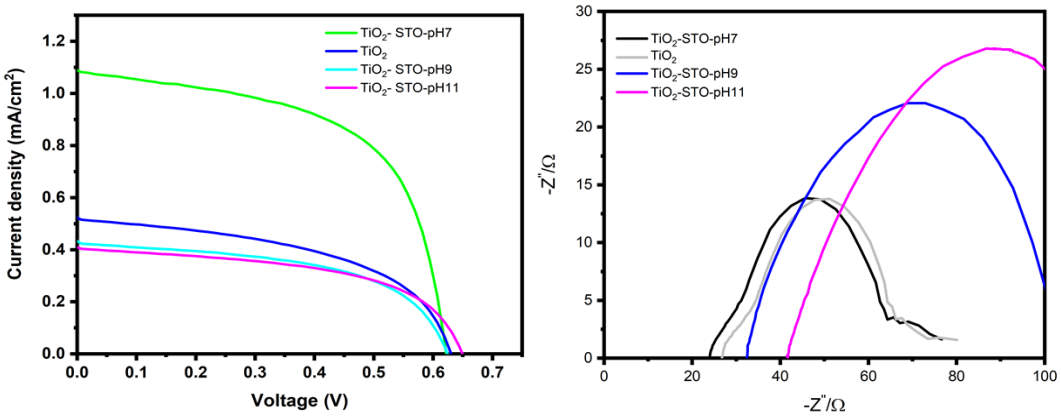

Fig. 6. (a) J-V and (b) Nyquist plot for TiO_2 and different pH of Sr_2TiO_4 decorated TiO_2.

Table 1. Comparative DSSC photovoltaic performance data were determined by J–V of TiO_2 and the different pH of Sr_2TiO_4 decorated TiO_2.

Cell	J_{sc} (mA/cm^2)	V_{oc} (V)	FF	η
P25-TiO_2	0.52	0.63	0.51	0.16
TiO_2- STO-pH7	1.09	0.62	0.59	0.40
TiO_2- STO-pH9	0.43	0.62	0.54	0.14
TiO_2- STO-pH11	0. 41	0.64	0.54	0.14

4. Conclusions

TiO_2 and Sr_2TiO_4-decorated TiO_2 were successfully synthesized using the reflux method, with varying concentrations of NaOH to adjust the pH. The optimal condition of DSSCs is when using TiO_2 combined with Sr_2TiO_4 at a pH of 7. In summary, integrating Sr_2TiO_4 with TiO_2 nanostructures shows great potential for enhancing the efficiency, stability, and reliability of DSSCs. By leveraging the unique properties of Sr_2TiO_4 and its synergistic interactions with TiO_2, researchers aim to develop advanced photoanode materials that feature improved reduced charge recombination and enhanced charge transport properties

Acknowledgments

This research was funded by King Mongkut's University of Technology North Bangkok. Contract no. KMUTNB-66-KNOW-08.

References

[1] Lee, C.-R., H.-S. Kim, N.-G. Park, Frontiers of Optoelectronics in China, 2011. **4**: p. 59-64; https://doi.org/10.1007/s12200-011-0205-2
[2] Zhao, D., et al., The Journal of Physical Chemistry C, 2008. **112**(22): p. 8486-8494; https://pubs.acs.org/doi/10.1021/jp800127x
[3] Vittal, R., K.-C. Ho, Renewable and Sustainable Energy Reviews, 2017. **70**: p. 920-935; https://doi.org/10.1016/j.rser.2016.11.273
[4] Shakeel Ahmad, M., A.K. Pandey, N. Abd Rahim, Renewable and Sustainable Energy Reviews, 2017. **77**: p. 89-108; https://doi.org/10.1016/j.rser.2017.03.129
[5] DiMarco, B.N., et al., ACS Applied Materials & Interfaces, 2020. **12**(21): p. 23923-23930; https://pubs.acs.org/doi/10.1021/acsami.0c04117?goto=supporting-info&articleRef=test
[6] Tiwana, P., et al., ACS Nano, 2011. **5**(6): p. 5158-5166; https://doi.org/10.1021/nn201243y
[7] Farooq, N., et al., Journal of King Saud University - Science, 2024. **36**(6): p. 103210; https://doi.org/10.1016/j.jksus.2024.103210
[8] Djurišić, A.B., et al., Physica Status Solidi (RRL) – Rapid Research Letters, 2016. **10**(4): p. 281-299; https://doi.org/10.1002/pssr.201600012
[9] Zhang, C., et al., The Journal of Physical Chemistry C, 2012. **116**(37): p. 19807-19813; https://doi.org/10.1021/jp304911u
[10] Liau, L.C.-K., W.-W. Dai, Colloids and Surfaces A: Physicochemical and Engineering Aspects, 2008. **320**(1-3): p. 68-73; https://doi.org/10.1016/j.colsurfa.2008.01.014
[11] Nakata, K., et al., Chemistry Letters, 2011. **40**(10): p. 1107-1109; https://doi.org/10.1246/cl.2011.1107
[12] Suárez, F.J., et al., Chemistry of materials, 2007. **19**(13): p. 3096-3098; https://pubs.acs.org/doi/10.1021/cm0707354
[13] Calatayud, D.G., M. Rodríguez, T. Jardiel, Boletín de la Sociedad Española de Cerámica y Vidrio, 2015. **54**(4): p. 159-165; https://doi.org/10.1016/j.bsecv.2015.07.001
[14] Zhang, H., et al., ChemistrySelect, 2017. **2**(11): p. 3282-3288; https://doi.org/10.1002/slct.201601346
[15] Kishore Kumar, D., et al., Materials Science for Energy Technologies, 2020. **3**: p. 472-481; https://doi.org/10.1016/j.mset.2020.03.003
[16] Saxena, V., D.K. Aswal, Semiconductor Science and Technology, 2015. **30**(6): p. 064005; https://dx.doi.org/10.1088/0268-1242/30/6/064005
[17] Ünlü, B., S. Çakar, M. Özacar, Solar Energy, 2018. **166**: p. 441-449; https://doi.org/10.1016/j.solener.2018.03.064
[18] Low, F.W., C.W. Lai, Renewable and Sustainable Energy Reviews, 2018. **82**: p. 103-125; https://doi.org/10.1016/j.rser.2017.09.024
[19] Lee, K.-M., V. Suryanarayanan, K.-C. Ho, Solar Energy Materials and Solar Cells, 2006. **90**(15): p. 2398-2404; https://doi.org/10.1016/j.solmat.2006.03.034
[20] Rho, W.-Y., et al., Journal of Solid State Chemistry, 2018. **258**: p. 271-282; https://doi.org/10.1016/j.jssc.2017.10.018
[21] Keshavarzi, R., et al., Langmuir, 2015. **31**(42): p. 11659-11670; https://doi.org/10.1021/acs.langmuir.5b02718
[22] Tian, H., et al., Journal of Materials Chemistry, 2011. **21**(3): p. 863-868; http://dx.doi.org/10.1039/C0JM02941F
[23] Urgessa, Z.N., et al., Journal of Alloys and Compounds, 2019. **798**: p. 249-256; https://doi.org/10.1016/j.jallcom.2019.05.298
[24] Wei, L., et al., Thin Solid Films, 2017. **639**: p. 12-21; https://doi.org/10.1016/j.tsf.2017.08.011
[25] Liu, S., et al., Solar Energy Materials and Solar Cells, 2024. **266**: p. 112679; https://doi.org/10.1016/j.solmat.2023.112679
[26] Ahmadi, S., et al., International Journal of Photoenergy, 2014. **2014**(1): p. 198734; https://doi.org/10.1155/2014/198734
[27] Govindaraj, R., et al., Bulletin of Materials Science, 2015. **38**(2): p. 291-296; https://doi.org/10.1007/s12034-015-0874-3

[28] Ikpesu, J.E., et al., Solar Energy, 2020. **206**: p. 918-934; https://doi.org/10.1016/j.solener.2020.05.002
[29] Pan, H., et al., Materials Horizons, 2020. **7**(9): p. 2276-2291; https://doi.org/10.1039/D0MH00586J
[30] Selyanin, I., et al., Chimica Techno Acta. 2020. Vol. 7.№ 4, 2020. **7**(4): p. 140-149; https://doi.org/10.15826/chimtech.2020.7.4.01
[31] Wang, J., et al., International Journal of Molecular Sciences, 2022. **23**(18): p. 10927; https://doi.org/10.3390/ijms231810927
[32] Kwak, B.S., et al., Scientific Reports, 2017. **7**(1): p. 16370; https://doi.org/10.1038/s41598-017-16605-w
[33] Makuła, P., M. Pacia, W. Macyk, ACS Publications. p. 6814-6817;
[34] Hossain, M.K., et al., Optik, 2018. **171**: p. 507-516; https://doi.org/10.1016/j.ijleo.2018.05.032
[35] Gnida, P., et al., Energy & Fuels, 2020. **34**(11): p. 14344-14355; https://pubs.acs.org/doi/10.1021/acs.energyfuels.0c02188